ELSEVIER

Inorganica Chimica Acta 225 (1994) 191–200

Inorganica Chimica Acta

Synthesis and electrochemical properties of oxo-bridged manganese dimers incorporating alkali and alkaline earth cations

Colin P. Horwitz*, Yangzhen Ciringh

Department of Chemistry, Rensselaer Polytechnic Institute, Troy, NY 12180-3590, USA

Received 8 March 1994

Abstract

The dimer $[(\mathbf{1})Mn^{III}]_2(\mu\text{-O})$ (**3**) was synthesized by oxygenation of the mononuclear Mn(II) complex in CH_3CN. The ligand used was 3,3′-17-crown-6-SAL-3-CH_3-OPHEN (**1**). Dimer **3** reacted with KPF_6 and $Ba(SO_3CF_3)_2$ in DMF forming $\mathbf{3}\cdot 2KPF_6$ and $\mathbf{3}\cdot 2Ba(SO_3CF_3)_2$ and these were isolated and characterized by spectroscopic and electrochemical means. All of the dimers participated in a reversible two-electron transfer process that produced the corresponding Mn^{II},Mn^{II} (μ-oxo) dimer. Inclusion of cations into the crown ether portions of the dimer caused that formal reduction potential of **3** to shift to more positive values: $E°$ (**3**) = −120 mV, CH_2Cl_2; $E°$ ($\mathbf{3}\cdot 2KPF_6$) = 0 mV, CH_3CN; $E°$ ($\mathbf{3}\cdot 2Ba(SO_3CF_3)_2$) = 180 mV, CH_3CN all versus SSCE. Results of UV–Vis experiments suggested that the shift in formal reduction potential was caused primarily by an electrostatic effect and not a perturbation of the d orbitals on the Mn(III) centers.

Keywords: Electrochemistry; Manganese complexes; Oxo complexes; Dinuclear complexes; Alkali cation complexes; Alkaline earth cation complexes

1. Introduction

The synthesis and characterization of oxo-bridged manganese clusters is of current interest [1] as structural, chemical and spectroscopic models of the active sites of some manganese dependent enzymes [2] are developed. There is an extensive literature on bimetallic compounds bridged by two oxygen ligands, but there are only a few reported examples of manganese dimers bridged by a single oxo ligand. The unsupported dimers schematically represented by **I**, are much less common [3] than those of type **II** [4], so their chemical and physical attributes are not well known. However, since a structure of this type may be a portion of the tetranuclear manganese core of the oxygen evolving complex (OEC) in photosystem II, and other manganese dependent enzymes [2,5], it is important to find the criteria necessary to form these model compounds and to determine their properties.

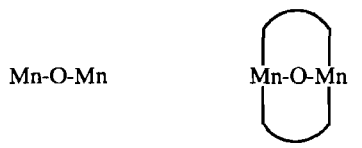

I II

In addition to synthesizing unsupported μ-oxo dimers, we wanted to examine the effect of alkali and alkaline earth cations on their physical properties because a Ca^{2+} ion is present in the OEC but its role has not been delineated. We are aware of only one example where alkaline earth cations have been deliberately included in a manganese–oxo cluster [6]. One possible function for Ca^{2+} in the OEC is to raise the redox potential of the metal center(s) allowing for a more facile water oxidation process. We show with relatively simple Schiff base compounds that this is a reasonable role to ascribe to the cation.

Reinhoudt and co-workers [7] recently reported that Schiff base ligands modified with crown ether moieties can simultaneously coordinate transition metal ions through the imine nitrogens and phenolate oxygens, and alkali and alkaline earth cations via the pendant crown ether group. We used this information to synthesize mononuclear Mn(II) and Mn(III) complexes that bound additional cations using the ligand, shown

*Corresponding author. Present address: Department of Chemistry, Carnegie Mellon University, Pittsburgh, PA 15213, USA.

SSDI 0020-1693(94)04047-Y

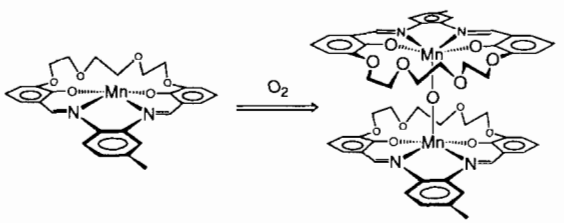

2 3

Scheme 1.

in Scheme 1. More importantly, we found that oxygenation of the Mn(II) complex, **2**, in CH_3CN resulted in formation of the neutral, singly oxo-bridged dimer, $[(\mathbf{1})Mn^{III}]_2(\mu\text{-}O)$ (**3**) (Scheme 1). Compound **3** reacts with KPF_6 and $BaTf_2$ producing $[(\mathbf{1})Mn^{III}]_2(\mu\text{-}O)\cdot 2KPF_6$ ($\mathbf{3}\cdot 2KPF_6$) and $[(\mathbf{1})Mn^{III}]_2(\mu\text{-}O)\cdot 2Ba(SO_3CF_3)_2$ ($\mathbf{3}\cdot 2BaTf_2$), respectively. The electron transfer properties of the dimers are truly unique compared to other dinuclear manganese compounds because they undergo a single two-electron reduction that is chemically and electrochemically reversible.

2. Experimental

2.1. Physical measurements

FT-IR spectra of solids (KBr disks) were taken using a Perkin-Elmer 1800 FTIR spectrometer while UV–Vis spectra were obtained using a Hewlett-Packard HP8452A diode array spectrophotometer. Thermogravimetric analyses (TGA) were performed on a Perkin-Elmer model series 7 thermal analysis system. Conductance measurements were made using a GenRad GR 1689M RLC Digibridge and a cell constructed at RPI. Elemental analyses were performed by Quantitative Technologies, Inc., Whitehouse, NJ. Mass spectral analyses were performed at New York University using a Vestec model 200 single quadrupole electrospray ionization mass spectrometer under the following conditions: needle voltage, 2.0–2.6 kV; flow rate, 3–5 microliter/min; ESI chamber temperature, 55–60 °C; repeller voltage, 20 V; block temperature, 200–300 °C; lens temperature, 110–115 °C. Sample solutions (1000 to 1 μM) were injected directly into the ESI chamber with a syringe pump (Sega Instruments, Inc.). Spectra were the average of about 10–20 scans.

2.2. Electrochemistry

Electrochemical measurements were made using an EG&G PAR model 273 potentiostat/galvanostat and recorded on a Graphtec WX-1200 XY recorder or a personal computer. Cyclic voltammograms, CVs, and differential pulse voltammograms, DPVs, were obtained in three compartment cells with a glassy carbon, GC, disk working electrode ($A \sim 0.071$ or 0.0078 cm^2), a Pt wire counter electrode and a SSCE (sodium chloride saturated calomel electrode) reference electrode. Rotating disk electrode voltammetry, RDEV, was performed using a Pine Instruments AFASR analytical rotator with a GC disk electrode ($A \sim 0.46$ cm^2). The supporting electrolyte was Bu_4NClO_4(TBAP) (Baker Analyzed).

2.3. Materials

The following reagent grade chemicals were used as received from Aldrich: NaH, 2,3-dihydroxybenzaldehyde, triethylene glycol ditosylate, $Mn(CH_3CO(O))_2\cdot 4H_2O$, 3,4-diaminotoluene and KPF_6. $Ba(SO_3CF_3)_2$, $BaTF_2$, was prepared according to the method of van Staveren et al. [7]. Cp_2Co (Strem) was purified by sublimation prior to use. $[Cp_2Fe][PF_6]$ was prepared by a method described in the literature [8]. The ligand (26-benzoyl-9,10,12,13,15,16-hexahydro-29,30-dihydroxy-3,7:18,22-dimethano-2,11,14,17,1,24-benzotetraoxadiazacyclohexacosine-O^8,O^{11},O^{14},O^{29},O^{30}), $\mathbf{1}(H)_2$ which we refer to as 3,3′-17-crown-6-SAL-3-CH_3-OPHEN in its deprotonated form, was prepared by the method of van Staveren et al. [7] and the purity checked by comparing its ^1H NMR spectrum with the values reported in the literature. CH_3CN, CH_2Cl_2, DMF and CH_3OH were purified by standard methods [9]. Air-sensitive compounds were prepared under an N_2 atmosphere using standard Schlenk techniques and stored in an N_2 filled glove box (Vacuum Atmospheres).

2.3.1. (3,3′-17-Crown-6-SAL-3-CH_3-OPHEN)Mn(II) (2)

To ligand $\mathbf{1}(H)_2$ (191 mg, 0.4 mmol) dissolved in deaerated CH_3OH (15 ml) was added $Mn(CH_3COO)_2\cdot 4H_2O$ (98 mg, 0.4 mmol) (dissolved in 10 ml CH_3OH) which produced an orange solution. The solution was refluxed for 30 min to insure complete reaction. No precipitate appeared at 20 °C so the solvent was removed in vacuo leaving an orange solid that was washed with copious quantities of H_2O to remove any residual acid. After drying, the solid was dissolved in CH_3CN, and then the solvent was removed in vacuo leaving an orange solid which was dried at 50 °C for 2 h (yield 85–90%).

Anal. Calc. for $C_{27}H_{26}N_2O_6Mn\cdot H_2O\cdot CH_3OH$: C, 58.03; H, 5.57; N, 4.83. Found: C, 58.03; H, 5.23; N, 4.77%. (Solvent molecules were detected by a TGA measurement: calc. (found) wt.% H_2O, 3.1 (3.2); CH_3OH, 5.5 (3.6)).

2.3.2. (3,3′-17-Crown-6-SAL-3-CH_3-OPHEN)Mn(III)-PF_6 ($2\cdot PF_6$)

Procedure A. Compound **2** (100 mg, 0.19 mmol) was dissolved in methanol then a four-fold molar excess of

NH_4PF_6 was added as a solid. Air was bubbled through this mixture until all the solid was consumed and a dark brown homogeneous solution remained. The volatiles were removed in vacuo and the solid was washed well with H_2O to remove residual salts. The residue was dissolved in CH_3CN, dried with Na_2SO_4, and then the solvent was removed yielding a black solid that was dried in vacuo at 20 °C overnight. Yield 91%.

Procedure B. Compound **2** (50 mg, 0.094 mmol) was dissolved in deoxygenated CH_3CN (10 ml) then an equimolar amount of $[Cp_2Fe][PF_6]$ was added. The mixture was stirred for 3 h under N_2 forming a homogeneous deep brown solution. Ether was added causing Cp_2Fe to precipitate. The CH_3CN/Et_2O mixture was removed in vacuo leaving a green–black powder. Yield 87%.

Anal. Calc. for $C_{27}H_{26}N_2O_6MnPF_6 \cdot 2H_2O$ using procedure A: C, 45.65; H, 4.26; N, 3.94. Found: C, 45.58; H, 4.21; N, 4.01%. (Solvent molecules were detected by a TGA measurement: calc. (found) wt.% H_2O, 5.1 (6.5).)

2.3.3. *[(3,3'-17-Crown-6-SAL-3-CH_3-OPHEN)Mn(III)]$_2$-(μ-O) (3)*

Compound **2** (50 mg, 0.094 mmol) was loaded in a single neck round bottom flask in the glove box, deoxygenated CH_3CN (15 ml) was added and the flask was sealed with a rubber septum. The flask was removed from the glove box and O_2 (or air) was bubbled through the solution for 15 min which caused the red–yellow solution to become brown and a brown precipitate formed. The solid was recovered by filtration through a medium porosity glass frit, washed with CH_3CN and dried in vacuo at 20 °C (yield 85–90%).

Anal. Calc. for $C_{54}H_{52}N_4O_{13}Mn_2 \cdot 1.5H_2O$: C, 58.86; H, 5.03; N, 5.08. Found: C, 58.96; H, 4.89; N, 5.13%. $\Lambda = 33$ cm^2 Ω^{-1} in DMF (a non-electrolyte).

2.3.4. *[(3,3'-17-Crown-6-SAL-3-CH_3-OPHEN)-Mn(III)]$_2$(μ-O)·2MX (3·2KPF$_6$ and 3·2BaTf$_2$)*

The procedures used for the preparation of **3**·2KPF$_6$ and **3**·2BaTf$_2$ were similar so only the one for **3**·2KPF$_6$ is detailed. Addition of KPF_6 (18.4 mg, 0.1 mmol) to a DMF (10 ml) solution of **3** (54 mg, 0.05 mmol) resulted in an immediate color change from brown to red–brown. After 15 min, diethyl ether was layered on the top of the DMF and allowed to diffuse slowly into the DMF producing small deep red–brown crystals. In the case of **3**·2BaTf$_2$, the product was a red–brown powder. Yield 80–90% in both cases.

Anal. Calc. for $C_{54}H_{52}F_{12}K_2Mn_2N_4O_{13}P_2 \cdot H_2O$ (**3**·2KPF$_6$): C, 44.39; H, 3.73; N, 3.83. Found: C, 44.36; H, 3.75; N, 3.57%. MS *m/z*: 1172 [**3**·2K·F]$^+$, 1078 [(**1**)Mn]$_2$F and 681 (see text). $\Lambda = 136$ cm^2 Ω^{-1} in DMF; Evans method $\mu_{eff} = 9.0$ BM. *Anal.* Calc. for $C_{58}H_{52}Ba_2F_{12}Mn_2N_4O_{25}S_4$ (**3**·2BaTf$_2$): C, 35.8; H, 2.69; N, 2.88. Found: C, 35.46; H, 3.01; N, 3.14%. $\Lambda = 312$ cm^2 Ω^{-1} in DMF; Evans method $\mu_{eff} = 8.69$ BM.

3. Results and discussion

3.1. Chemical and physical studies: compounds 2 and 2·PF$_6$

The chemical and physical properties of compounds **2**, **2**·PF$_6$ and their cation containing derivatives are presented first because this permits us to compare and contrast details of the mononuclear compounds with those of the dimers. It will be seen that many physical features of the compounds are similar.

3.1.1. Compounds 2

The 3,3'-17-crown-6-SAL-3-CH_3-OPHEN ligand in its protonated form, (**1**)H$_2$, readily reacts with $Mn(CH_3CO(O))_2 \cdot 4H_2O$ in refluxing methanol producing the air-sensitive complex (**1**)Mn^{II}, (**2**) in high yield. The nearly identical electronic spectra of **2** and other (SALOPHEN)Mn^{II} type complexes [10] suggests similar environments for the metal centers. Compound **2** readily complexed alkali and alkaline earth cations such as Li^+, Na^+, K^+, Ca^{2+} and Ba^{2+} (M^{n+}) in CH_3CN. UV–Vis and electrochemical experiments revealed that cation uptake occurred in a rigorous 1:1 M^{n+}:**2** ratio (addition of an excess of the cation produced no changes in the absorption spectrum or the formal reduction potential for the complex beyond those observed upon incorporation of 1 equiv. of the cation).

Inclusion of the cation caused the absorption bands in the electronic spectrum assignable to ligand based transitions, π–π^* of the arenes and of the imines, and charge transfer bands [11] to shift slightly in energy when compared to **2**, Table 1. The shape and intensity of the absorption bands were the same for **2** and its cationic derivatives. Na^+ and K^+ cations caused a bathochromic shift in these absorptions while the other cations resulted in a hypsochromic shift. This behavior is different from that reported for the interaction of alkali cations with (SALEN)Ni^{II} complexes [12] where all of the transitions moved to higher energy upon

Table 1
UV–Vis properties of **2** and its salt complexes in CH_3CN

Compound	λ (nm) ($\epsilon \times 10^{-3}$ (M^{-1} cm^{-1}))
2	248 (27.1), 302 (18.4), 342 (sh)[a], 390 (9.21)
2·$LiClO_4$	246, 304, 338 (sh), 386
2·$NaPF_6$	248, 308, 344 (sh), 392
2·KPF_6	248, 308, 346 (sh), 396
2·$CaTf_2$	242, 304, 342 (sh), 376
2·$BaTf_2$	246, 306, 342 (sh), 384

[a]sh = shoulder.

cation association. The inconsistent energy shift observed here may be rationalized by differences in the geometry of the crown ether for each cation, different ion pairing phenomena or solvation effects, and possibly other factors.

3.1.2. Compound $2 \cdot PF_6$

The green–black Mn(III) compound $\mathbf{2} \cdot PF_6$ was synthesized by exposing a methanol solution containing **2** to O_2, Eq. (1) and Table 2. The identical complex, as determined by electrochemical and spectroscopic means, formed upon oxidation of **2** with $[Cp_2Fe][PF_6]$ in CH_3CN under N_2. Oxidation results in loss of the absorption band in the 390 nm region and appearance of a new broad absorption band centered around 600 nm ($\epsilon = 95$ M^{-1} cm^{-1}). Based on the molar absorptivity, this absorption most likely arises from a d → d type transition [11].

$$(\mathbf{1})Mn^{II} + O_2 \xrightarrow{CH_3OH} [(\mathbf{1})Mn^{III}]^+ \quad (1)$$

Compound $\mathbf{2} \cdot PF_6$ also reacts with all of the cations investigated in a strict 1:1 M^{n+}:$\mathbf{2} \cdot PF_6$ molar ratio in CH_3CN as determined by electrochemical and UV–Vis experiments. This 1:1 M^{n+}:$\mathbf{2} \cdot PF_2$ ratio is interesting because Li^+ usually prefers a crown ether with a smaller binding cavity [13] and inclusion of Ba^{2+} and Ca^{2+} produces tricationic species. All of the cations caused a shift to lower wavelength for absorptions from ligand and charge transfer transitions, Fig. 1.

The d → d transitions provide information about the d orbital energies at the Mn(III) center. As shown in the insert in Fig. 1 the absorption at 600 nm for $\mathbf{2} \cdot PF_6$ does not shift substantially in energy upon Ba^{2+} incorporation but it does decrease in intensity. Similar effects are observed for the other cations. The broad nature of this absorption band limits interpreting these small changes. It is possible that other d → d transitions that should be present for an Mn^{III} ion coordinated in a Schiff base ligand [11] do shift but they may have been masked by more intense transitions from the ligand or occurred at energies lower than the limit of the spectrophotometer.

In contrast to the small changes in the electronic spectrum, the formal potential for the $Mn^{III/II}$ couple in $\mathbf{2} \cdot PF_6$ under N_2 is strongly influenced by the cations, Table 2 and Fig. 2. The predominant cause for the shift in the formal potential upon cation incorporation is an electrostatic one [14,15] as application of Eq. (2) successfully accounts for the majority of the change.

$$\Delta E = -q_1 q_2 / 4\pi\epsilon K r \quad (2)$$

ΔE is the difference in formal potentials of $\mathbf{2} \cdot PF_6$ and the cation complex, $q_1 = 1$, q_2 = cation charge, ϵ = permittivity of a vacuum, $K = 36$, dielectric constant of CH_3CN, and $r = 3.6$ Å, the cation to transition metal distance observed in analogous Schiff base compounds [16].

3.2. Chemical and physical properties of dimers 3, $3 \cdot 2KPF_6$ and $3 \cdot 2BaTf_2$

Exposure of a CH_3CN solution of **2** to O_2 resulted in precipitation of $[(\mathbf{1})Mn^{III}]_2(\mu\text{-}O)$ (**3**), a brown solid, Eq. (3) and Scheme 1. We observed for other Mn(II) Schiff base complexes that oxygenation in an aprotic solvent produced oxo-bridged dimers [17–19]. Reaction of **3** with 2 molar equiv. of KPF_6 or $BaTf_2$ in DMF yields $\mathbf{3} \cdot 2KPF_6$ or $\mathbf{3} \cdot 2BaTf_2$, respectively. We have been unable to obtain X-ray quality single crystals of the dimers so far but combustion analytical data, mass spectroscopic data and reactivity studies obtained for the complexes are consistent with their given formulations. In addition, conductance measurements in DMF reveal that **3** is non-ionic, $\mathbf{3} \cdot 2KPF_6$ is a 1:2 electrolyte and $\mathbf{3} \cdot 2BaTf_2$ is a 1:4 electrolyte.

$$(\mathbf{1})Mn^{II} + O_2 \xrightarrow{CH_3CN} [(\mathbf{1})Mn^{III}]_2(\mu\text{-}O) \quad (3)$$

Table 2
Electrochemical and UV–Vis properties of $\mathbf{2} \cdot PF_6$ and its salt complexes

Compound	Solvent	E° vs. SSCE[a] (mV)	ΔE_p[b] (mV)	K_2/K_1	λ (nm) ($\epsilon \times 10^{-3}$ (M^{-1} cm^{-1}))
$\mathbf{2} \cdot PF_6$	CH_3CN	−45	90		264 (36.2); 314 (22.2); 370 (22.8); 480 (4.4)
$\mathbf{2} \cdot PF_6$	DMF	−90			
$\mathbf{2} \cdot PF_6 \cdot LiClO_4$	CH_3CN	55	180	50	236; 306; 362; 464
$\mathbf{2} \cdot PF_6 \cdot KPF_6$	CH_3CN	25	85	15	246; 308; 362; 462
$\mathbf{2} \cdot PF_6 \cdot CaTf_2$	CH_3CN	245	115	8.0×10^4	228; 304; 364; 430
$\mathbf{2} \cdot PF_6 \cdot BaTf_2$	CH_3CN	200	105	1.4×10^4	224; 296; 356; 436

[a]0.1 M $TBAClO_4$, GC working electrode.
[b]Measured at 50 mV s^{-1}.
[c]$K_2/K_1 = \exp(-nF(E_f^\circ - E_c^\circ)/RT)$ where n = number of electrons, $n = 1$; E_f° = formal reduction potential of cation free complex; E_c° = formal reduction potential of the cation containing complex; $T = 298$ K; F and R have their usual meaning (see Ref. [39]).

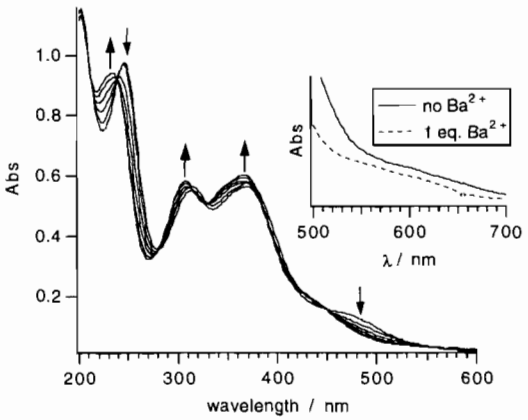

Fig. 1. Titration of $[(\mathbf{1})Mn^{III}]^+$ (0.07 μmol) with $Ba(SO_3CF_3)_2$ (20.0 μl aliquots; 3.5 mM solution) in CH_3CN as monitored by UV–Vis spectroscopy. Insert is a higher concentration of $[(\mathbf{1})Mn^{III}]^+$ emphasizing the d→d transition.

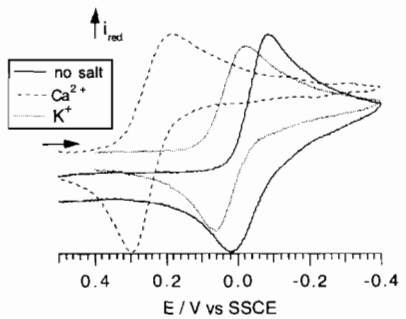

Fig. 2. Cyclic voltammograms of $\mathbf{2}\cdot PF_6$, $\mathbf{2}\cdot PF_6\cdot K^+$ and $\mathbf{2}\cdot PF_6\cdot Ca^{2+}$ under N_2. Experimental conditions: $v = 50$ mV s^{-1}, 0.1 M $TBAClO_4$/CH_3CN, GC electrode.

3.3. Spectroscopic characterization

3.3.1. IR spectroscopy

IR spectra of the dimers **3** and $\mathbf{3}\cdot 2KPF_6$ and the mononuclear complex $\mathbf{2}\cdot PF_6$ are essentially identical in the 1000–450 cm^{-1} region (ignoring PF_6 bands). However, there is a weak band around 650 cm^{-1} detected in both **3** and $\mathbf{3}\cdot 2KPF_6$ that is absent in $\mathbf{2}\cdot PF_6$ (the strong absorption from the SO_3CF_3 anion masks this region for $\mathbf{3}\cdot 2BaTf_2$). The similar IR spectra demonstrate that no significant changes occur in the coordination geometry at the metal center of the planar ligand structure upon dimerization [17–21]. The band at 650 cm^{-1} is in a region where metal oxo stretches are expected to occur [22]. Isotopic labeling experiments and Raman spectroscopic studies are planned to determine if this band is associated with the $Mn_2(\mu\text{-}O)$ core.

3.3.2. UV–Vis spectroscopy

The UV–Vis spectra of **3** and $\mathbf{2}\cdot PF_6$ are similar with regard to band positions and intensities, Tables 2 and 3. This was not completely unexpected since the ligand field strength of the O^{2-} ligand is about equal to that of water [23]. The Mn(III) center in $\mathbf{2}\cdot PF_6$ is likely to be coordinated by either solvent molecules (CH_3CN in this case) or H_2O molecules (see the analysis of $\mathbf{2}\cdot PF_6$) so the spectra of $\mathbf{2}\cdot PF_6$ and **3** should probably be similar [19,24]. Inclusion of K^+ and Ba^{2+} into the crown ether caused a hypsochromic shift of the ligand and charge transfer absorption bands compared to the starting material, Table 3.

3.3.3. Mass spectroscopy

In the electrospray mass spectrum, positive ion detection mode, of $\mathbf{3}\cdot 2KPF_6$ dissolved in CH_3CN neither $[\mathbf{3}\cdot 2K\cdot PF_6]^+$ (*m/z* 1298) nor $[\mathbf{3}\cdot 2K]^{2+}$ (*m/z* 576) was detected. Rather the species observed was the μ-oxo dimer with a fluoride ion, $[\mathbf{3}\cdot 2K\cdot F]^+$, *m/z* 1172. In addition, a dimer devoid of K^+ cations and the oxo ligand but containing a fluoride ligand was detected at *m/z* 1078 $[[(\mathbf{1})Mn^{III}]_2F]^+$. Fluoride abstraction from PF_6 occurs for other Schiff base complexes having this anion as shown by electrospray mass spectroscopy [10] and it has been observed under more typical reaction conditions for a variety of coordination compounds [25]. The most intense peak in the spectrum is found at *m/z* 681. This can be accounted for either by formation of a monovalent cation in which fragmentation of the crown ether portion of the ligand occurred and solvent molecules are bound to the cation, structure **III**, or by association of an adventitious Na^+ cation and a solvent molecule to the dimer with formation of a divalent species, $[\mathbf{3}\cdot 2K\cdot Na\cdot PF_6\cdot CH_3CN]^{2+}$ (**IV**). Cation association/exchange processes have been observed for other crown ether Schiff base compounds that we have examined by electrospray mass spectroscopy [26] so at this time we favor structure **IV**.

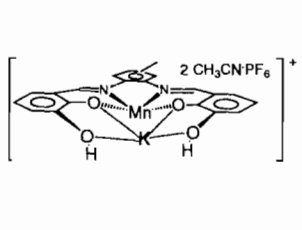

III

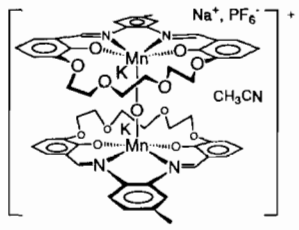

IV

3.4. Reactivity. Oxygen atom transfer

Our chemical evidence for the μ-oxo formulation comes from a study of the reactivity of the dimers toward $(SALEN)Fe^{II}(L'Fe^{II})$. We previously showed that oxo-bridged manganese dimers like $[LMn^{IV}(\mu\text{-}O)]_2$ (L is a tetradentate Schiff base ligand) [17,27] undergo facile *complete* oxygen atom transfer reactions [28,29] with $(SALEN)Fe^{II}$, Eq. (4). The important feature of the reaction is that it is stoichiometric in both $(SALEN)Fe^{II}$ and the manganese dimer which allows an accurate determination of the number of oxygen

Table 3
Electrochemical and UV–Vis properties of **3** and **3**·2MX

Compound	Solvent	$E°$ vs. SSCE[a] (mV)	K_2/K_1[b]	λ (nm) ($\epsilon\times10^{-3}$ (M^{-1} cm^{-1}))
3	CH_2Cl_2	−120		310 (31.9); 368 (27.5); 474 (9.5)
3	DMF	−100		
3·2KPF$_6$	CH_3CN	0		242 (59.6); 310 (33.1); 362 (35.6); 458 (10.9)
3·2KPF$_6$	DMF	0	48[c]	
3·2BaTf$_2$	CH_3CN	180		238 (55.1); 304 (33.8); 360 (37.5); 444 (10.9)
3·2BaTf$_2$	DMF	190	7.5×10^3[c]	

[a]0.1 M $TBAClO_4$, GC working electrode.
[b]See Ref. [39] using $n=1$ since the electron transfer is two one-electron reductions.
[c]Calculated using the $E_f°$ determined for **3** in DMF.

atoms in the manganese complex. This multi-electron inner-sphere type electron transfer reaction uses as its driving force the formation of the iron oxo dimer.

$$[LMn^{IV}(\mu\text{-}O)]_2 + 4L'Fe^{II} \longrightarrow 2LMn^{II} + 2[L'Fe^{III}]_2(\mu\text{-}O) \quad (4)$$

Oxygen atom transfer chemistry applied to compound **3** revealed that 2.0 molar equiv. of (SALEN)Fe^{II} were consumed per mole of **3**, Eq. (5). Fig. 3 shows the changes that occur in the UV–Vis spectrum upon oxo transfer. Observation of the isosbestic points indicates that there are no long lived intermediates during the oxygen atom transfer process. Formally, Eq. (5) corresponds to a one oxygen atom, two-electron transfer process. As there is no evidence for dissociation of **3** into mononuclear fragments, the chemistry in Eq. (5) is another example of a bridging oxo ligand directly participating in an oxygen atom transfer process, suggesting that this may be a more common inner-sphere electron transfer pathway than previously thought.

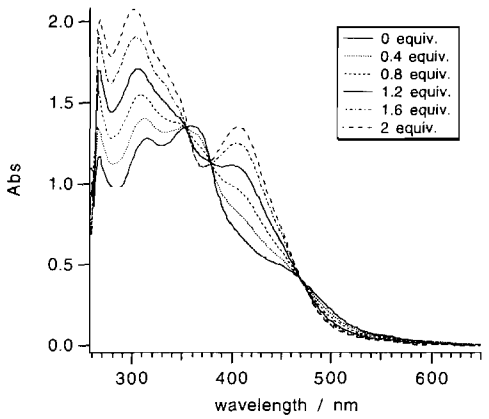

Fig. 3. Reaction of [(**1**)Mn^{III}]$_2$(μ-O) (0.094 μmol) with (SALEN)Fe^{II} (2.0 μl aliquots of a 9.44 mM solution) in DMF as monitored by UV–Vis spectroscopy.

$$[(\mathbf{1})Mn^{III}]_2(\mu\text{-}O) + 2L'Fe^{II} \longrightarrow \underset{\mathbf{3}}{} \quad 2(\mathbf{1})Mn^{II} + [L'Fe^{III}]_2(\mu\text{-}O) \quad (5)$$
$$\mathbf{2}$$

The oxygen atom transfer reaction was not entirely successful with **3**·2KPF$_6$ or **3**·2BaTf$_2$ because (SALEN)Fe^{II} acted as an outer-sphere electron transfer agent. The steric effect arising from the presence of the cations and their associated solvent molecules limiting the approach of the iron reagent to the oxo ligand and the positive shift in formal reduction potentials for the cation containing complexes compared to **3** makes them more easily reduced, see below, are two likely explanations for this behavior. However, oxygen atom transfer did occur to some extent with these dimers confirming the presence of the oxo ligand in both **3**·2KPF$_6$ and **3**·2BaTf$_2$.

3.5. Electron transfer properties

All of the dimers exhibited a single, electrochemically and chemically reversible two-electron transfer process, Table 3 and Eq. (6). The electrochemical reversibility

$$[(\mathbf{1})Mn^{III}]_2(\mu\text{-}O) + 2e^- \rightleftharpoons [(\mathbf{1})Mn^{II}]_2(\mu\text{-}O)]^{2-} \quad (6)$$

and the potential shifts that result upon cation insertion are illustrated by the CVs in Fig. 4. We describe below results of a chemical reduction of the dimer with Cp_2Co and an RDE experiment that illustrate the two-electron reduction process. CV and DPV experiments are used to show that the electron transfer events correspond to two one-electron reductions.

The multi-electron reduction is a unique property of these dimers as the Mn^{III},Mn^{III}(μ-oxo) (μ-carboxylato) complexes [30] commonly exhibit irreversible one-electron reductions but reversible or quasi-reversible one-electron oxidations. Only one of the carboxylato

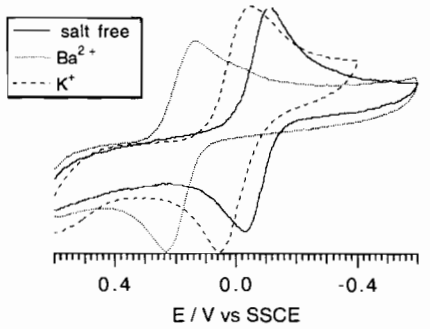

Fig. 4. Cyclic voltammograms of **3**, **3**·2KPF$_6$ and **3**·2Ba(SO$_3$CF$_3$)$_2$ under N$_2$. Experimental conditions: $v = 50$ mV s^{-1}, 0.1 M TBAClO$_4$/CH$_3$CN, GC electrode.

bridged dimers [31] has a two-electron reduction but this irreversibly decomposed the dimer. There are no reported electrochemical studies on the other unsupported manganese μ-oxo dimers.

3.6. Chemical reduction

We recently reported that [(SALEN)Mn^{IV}(μ-O)]$_2$ exhibited reversible electrochemical behavior on a short experimental time scale (CV) but on a longer time scale (bulk electrolysis) the compound was unstable due to loss of one oxo ligand with apparent formation of the corresponding μ-oxo dimer [17]. It was important then to determine if a similar situation applied to the dimers reported here. The following three experiments provide the evidence for stability of the dimer. First, a reduction/oxidation cycle of **3**·2BaTf$_2$ was performed under N$_2$ and this was monitored by UV–Vis spectroscopy. Reduction of **3**·2BaTf$_2$ with Cp$_2$Co resulted in the appearance of an absorption band at $\lambda = 392$ nm, an energy similar to that for **2**·BaTf$_2$, Table 1, and four isosbestic points, $\lambda = 238$, 330, 386 and 436 nm, Fig. 5(a). The absorption band at 362 nm stopped decreasing in intensity after 2 molar equiv. of Cp$_2$Co were consumed, Fig. 5(b). This reduced dimer was then oxidized with 2 equiv. of [Cp$_2$Fe]$^+$ which produced a spectrum nearly identical to the starting material, Fig. 5(a) inset (the mismatch in intensities at high energy is due to the presence of Cp$_2$Fe and [Cp$_2$Co]$^+$ in solution). Second, a sample of **3** that had undergone the reduction/oxidation cycle with Cp$_2$Co and [Cp$_2$Fe]$^+$ was still capable of transferring its oxo ligand to (SALEN)Fe^{II} as in Eq. (5). Finally, a particularly remarkable feature of the reduced dimer is its air stability. The UV–Vis spectrum of a CH$_3$CN solution of the reduced form of **3**·2BaTf$_2$ exposed to air showed no changes over 1 h and only minimal changes after 6 h. If the oxo ligand had been expelled to form the mononuclear Mn(II) complex, oxidation back to the μ-oxo dimer should have occurred within 5 min of air exposure.

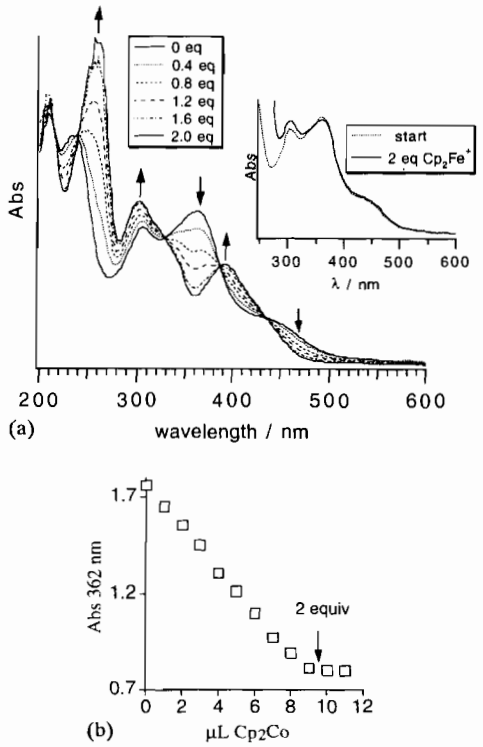

Fig. 5. (a) Reduction of **3**·2Ba(SO$_3$CF$_3$)$_2$ (0.11 μmol) with Cp$_2$Co (1.0 μl aliquots of a 22.4 mM solution) in CH$_3$CN under N$_2$ as monitored by UV–Vis spectroscopy. The inset shows spectra of the starting compound and the compound present following reduction with 2 equiv. of Cp$_2$Co and then reoxidation with 2 equiv. of [Cp$_2$Fe]$^+$. (b) Plot of the diminution of the absorption at $\lambda = 362$ nm vs. the quantity of Cp$_2$Co added.

3.7. Electrochemical properties

RDE voltammetry

There is a recent report of an oxo-bridged V(IV) dimer with SALEN ligands [(SALEN)V^{IV}]$_2$(μ-O) that undergoes at two-electron transfer but this is due to a disproportionation reaction, Eq. (7) [32]. A similar situation could easily be envisioned here as mixed valent μ-oxo dimers like those in Eq. (8) are known for the supported oxo-bridged dimers. RDEV was used to show that such a reaction did not occur for **3** and its derivatives. RDEV was also used to confirm that two reducing equivalents were consumed during the reduction of **3**·2KPF$_6$ by comparing the slope from a Levich plot for this compound to the one found for **2**·PF$_6$·KPF$_6$ at the same concentration [32,33]. The Levich plot is i_{lim} versus $\omega^{1/2}$ where i_{lim} is the current on the limiting current plateau and ω is the electrode rotation rate.

$$2[LV^{IV}]_2(\mu\text{-O}) \longrightarrow [[L_2V^{III},V^{IV}](\mu\text{-O})]^- + [[L_2V^{IV},V^{V}](\mu\text{-O})]^+ \quad (7)$$

L = SALEN

$$2[(\mathbf{1})Mn^{III}]_2(\mu\text{-}O) \longrightarrow [[(\mathbf{1})_2Mn^{III},Mn^{II}](\mu\text{-}O)]^- + [[(\mathbf{1})_2Mn^{III},Mn^{IV}](\mu\text{-}O)]^+ \quad (8)$$

A disproportionation is readily discounted since the voltammograms shown in Fig. 6(a) have currents starting at nearly 0 μA at all rotation rates and no crossing of current–potential curves occurs at any rotation rate. The Levich plot, Fig. 6(b), gives a ratio of slopes of 1.7 which is close to the predicted 2.0 value. If different diffusion coefficients are accounted for $\mathbf{6}\cdot KPF_6$, $D_0 = 1.05\times10^{-5}$ cm^2 s^{-1}, and $\mathbf{3}\cdot 2KPF_6$, $D_0 = 8.8\times10^{-6}$ cm^2 s^{-1}, the ratio is 2.0. These two RDE results reveal that the electron transfer reaction for the oxo dimers is the one depicted in Eq. (6).

3.7.2. CV and DPV

Since disproportionation did not occur, we wanted to understand how the individual electron transfer events took place. If we apply to the dimers here the widely used Dunitz–Orgel model for bonding in bridged dinuclear complexes [34], the d_{z^2} orbital on each metal ion is expected to lie highest in energy and to be empty in the Mn(III) form. The reduction processes correspond to addition of electrons to the d_{z^2} orbitals which could couple to each other through the bridging oxygen p_z orbital. This situation gives rise to at least two electron transfer scenarios. In the first, addition of an electron to one metal center results in the second one being added more easily, E_2° is less negative than E_1° ($E_2^\circ < E_1^\circ$). In the second, the presence of the first electron is felt in a repulsive sense at the second metal center so it is more difficult to add the second electron, i.e. E_2° is more negative than E_1° ($E_2^\circ \geqslant E_1^\circ$). The repulsive effect would be small here because only one redox process is observed. It has recently been reported that the oxo-bridged complex $[\{1\text{-methylimidazole})_3Ru\}_2(\mu\text{-}O)(\mu\text{-}O_2CCH_3)_2]^{2+}$ has $E_2^\circ < E_1^\circ$ [35] which is accompanied by some significant structural changes.

The electron transfer problem was addressed by CV and DPV experiments. Solutions of $\mathbf{2}\cdot PF_6$ and $\mathbf{3}\cdot 2BaTf_2$ both containing Cp_2Fe, the standard for a one-electron couple, were used for this study. For the CV experiment, the ΔE_p values were measured and compared. Although somewhat inconclusive, the results were most consistent with $E_2^\circ \geqslant E_1^\circ$ for the dimer. The DPV data analyzed using the $90/n$ relationship for the full width at half maximum, E_{fwhm}, were more informative as this value was nearly the same for Cp_2Fe ($E_{fwhm} = 90$ mV), $\mathbf{2}\cdot PF_6$ ($E_{fwhm} = 118$ mV) and $\mathbf{3}\cdot 2BaTf_2$ ($E_{fwhm} = 106$ mV). Thus reduction of the dimers is best described as two uncoupled or lightly coupled electron transfers. Unfortunately since we do not yet know structural details about the dimers, explaining this result now would be speculative at best.

3.8. Formation of 3·2MX

The final aspect of this study to be described was a determination of the equilibrium constants for the reactions in Eq. (9). A sample of **3** was titrated with $BaTf_2$ and the reaction monitored by UV–Vis and electrochemical methods. Results from a UV–Vis experiment are shown in Fig. 7. The changes to the spectrum are small, but the two isosbestic points at 378 and 426 nm indicate that there are only two absorbing species of appreciable concentration present

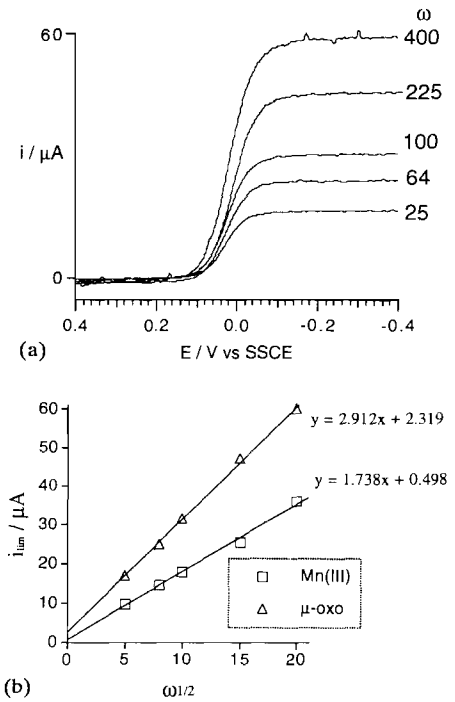

Fig. 6. (a) Rotating disk electrode voltammograms of $\mathbf{3}\cdot 2KPF_6$ (0.19 mM in 0.1 M $TBAClO_4/CH_3CN$) at the rotation rates indicated on the Figure. (b) Levich plot comparing the i_{lim} values for $\mathbf{3}\cdot 2KPF_6$ and $\mathbf{2}\cdot PF_6\cdot KPF_6$ at the rotation rates indicated on the Figure: both are 0.19 mM in 0.1 M $TBAClO_4/CH_3CN$.

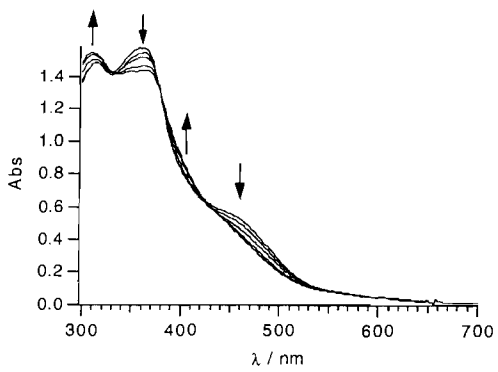

Fig. 7. Titration of $[(\mathbf{1})Mn^{III}]_2(\mu\text{-}O)$ (0.027 μmol in CH_3CN) with $Ba(SO_3CF_3)_2$ (2.0 μl aliquots of a 2.72 mM solution) in CH_3CN as monitored by UV–Vis spectroscopy.

under the reaction conditions. This was a preliminary indication that the mono-barium complex existed only at extremely low concentrations.

$$[(\mathbf{1})Mn^{III}]_2(\mu\text{-}O) + MX \overset{K_1}{\rightleftharpoons}$$

$$[(\mathbf{1})Mn^{III}]_2(\mu\text{-}O)\cdot MX + MX \overset{K_2}{\rightleftharpoons} \quad (9)$$

$$[(\mathbf{1})Mn^{III}]_2(\mu\text{-}O)\cdot 2MX$$

In order to analyze the electrochemical data, the formal reduction potential for a $\mathbf{3}\cdot Ba^{2+}$ intermediate was assumed to be 50 mV, the midpoint between those for **3** and $\mathbf{3}\cdot 2Ba^{2+}$, Table 3. As shown in Fig. 8(a), no clearly discernible redox process with a formal potential at 50 mV was observed throughout the entire titration procedure. The reduction marked with an asterisk (*) on Fig. 8 does not, we believe, arise from a $\mathbf{3}\cdot Ba^{2+}$ complex because this same reduction process was observed for an isolated sample of $\mathbf{3}\cdot 2Ba^{2+}$ in DMF. Furthermore, $\mathbf{3}\cdot 2BaTf_2$ is a 1:4 electrolyte in this solvent. More importantly, the observation of an isopotential point at $E = -80$ mV indicates the presence of only two electroactive species of reasonable concentration, **3** and $\mathbf{3}\cdot 2Ba^{2+}$. This experiment supports the UV–Vis experiment shown in Fig. 7.

Further corroboration for the predominant species being **3** and $\mathbf{3}\cdot 2Ba^{2+}$ comes from plotting the peak currents measured for reduction of $\mathbf{3}\cdot 2Ba^{2+}$ in solution, $i_{p,\,meas}$, and those calculated assuming 100% conversion of **3** to $\mathbf{3}\cdot 2Ba^{2+}$ upon each addition of $BaTf_2$, $i_{p,\,calc}$, versus the total quantity of $BaTf_2$ added, Fig. 8(b). The $i_{p,\,calc}$ values were determined using the equation for linear sweep voltammetry [33]. It can be seen that $i_{p,\,meas}$ and $i_{p,\,calc}$ were nearly identical up to 1.75 equiv. of added Ba^{2+} and then $i_{p,\,meas}$ was slightly lower than $i_{p,\,calc}$. We do not know why the last measured values were low, but the overall agreement between $i_{p,\,meas}$ and $i_{p,\,calc}$ is excellent. We conclude from these titration experiments that $K_2 \gg K_1$ and furthermore, suggest the possibility that uptake of the second cation is enhanced by the presence of the first. At this time there is not an obvious reason for this behavior.

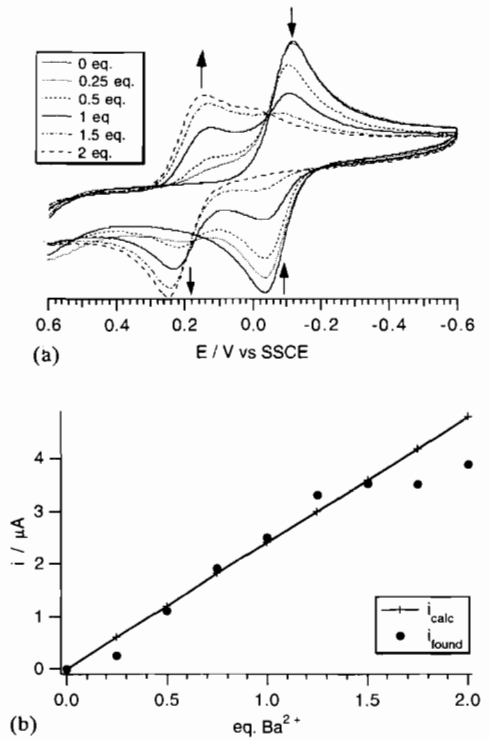

Fig. 8. (a) CVs recorded for the reaction of **3** (1.27 μmol) with $Ba(SO_3CF_3)_2$ (24.0 μl aliquots of a 13.1 mM solution). Experimental conditions: $v = 50$ mV s^{-1}, 0.1 M $TBAClO_4$/DMF, GC electrode. (b) Plot of $i_{p,\,meas}$ and $i_{p,\,calc}$ vs. the quantity of $Ba(SO_3CF_3)_2$ added. See text for details.

4. Conclusions

Our previous studies on Mn^{IV},Mn^{IV} bis(μ-oxo) dimers with Schiff base ligands [17–19,27] lead us to hypothesize that flexibility of the ligand would be a key factor to consider for stability of the dimer. This was based on our report that $[(SALEN)Mn^{IV}(\mu\text{-}O)]_2$ spontaneously lost an oxo ligand and formed the corresponding μ-oxo dimer while the analogous compounds derived from the more flexible 1,3-diaminopropane appear to be indefinitely stable in the bis(μ-oxo) form. It was expected then that oxygenation of (SALOPHEN)Mn(II) type compounds would allow isolation of a μ-oxo dimer [36]. Prior to the current investigation, reaction of (SALOPHEN)Mn(II) with O_2 had been reported to produce (SALOPHEN)Mn^{III}–OH [37,38] but the data presented here are more consistent with the generation of a neutral μ-oxo dimer. Thus our assumption about the role of backbone rigidity playing a role in the formation of μ-oxo dimers appears to be correct for the Schiff base compounds.

As noted in Section 1, the properties of unsupported μ-oxo dimers of manganese are not well known. We have found in this study that μ-oxo dimers with Schiff base ligands have unique electron transfer properties. Since an X-ray crystal structure of the dimers is not available, we cannot provide a good explanation for the observed behavior. Interestingly, while a cation placed close to the manganese center has a substantial effect on the formal potential of the complex it does not influence the overall electron transfer properties of the compounds. Finally, the substantial shifts in formal reduction potentials observed upon cation incorporation lend strong support to the notion that the cation functions to enhance the oxidizing power of the metal centers in the oxygen evolving complex of photosystem II.

Acknowledgements

We acknowledge the generous support of the National Science Foundation (Grant No. CHE-9200574). We thank Professors J.T. Warden for insightful discussions, G.E. Wnek for use of the Digibridge and K.E. Nash for her help in obtaining the conductance data.

References

[1] G. Christou and J.B. Vincent, in L. Que, Jr. (ed.), *Metal Clusters in Proteins,* ACS Symposium Series 372, American Chemical Society, Washington, DC, 1988; H.H. Thorp and G.W. Brudvig, *New. J. Chem., 15* (1991) 479; L. Que, Jr. and A.E. True, *Prog. Inorg. Chem., 38* (1990) 97.

[2] K. Wieghardt, *Angew. Chem., Int. Ed. Engl., 28* (1989) 1153; G.C. Dismukes, in J. Reedijk (ed.), *Bioinorganic Catalysis,* Marcel Dekker, New York, 1993, Ch. 10, p. 317.

[3] R.F. Ziolo, R.H. Stanford, G.R. Rossman and H.B. Gray, *J. Am. Chem. Soc., 96* (1974) 7910; L.H. Vogt, A. Zalkin and D.H. Templeton, *Inorg. Chem., 6* (1967) 1725; B.C. Schardt, F.J. Hollander and C.L. Hill, *J. Am. Chem. Soc., 104* (1982) 3964; J.A. Smegal, B.C. Schardt and C.L. Hill, *J. Am. Chem. Soc., 105* (1983) 3510; M.J. Camenzid, B.C. Schardt and C.L. Hill, *Inorg. Chem., 23* (1984) 1984; N. Kitajima, M. Osawa, M. Tanaka and Y. Morooka, *J. Am. Chem. Soc., 113* (1991) 8952.

[4] J.B. Vincent, H.-L. Tsai, A.G. Blackman, S. Wang, P.D.W. Boyd, K. Folting, J.C. Huffman, E.B. Lobkovsky, D.N. Hendrickson and G. Christou, *J. Am. Chem. Soc., 115* (1993) 12353, and refs. therein.

[5] G.W. Brudvig and R.H. Crabtree, *Prog. Inorg. Chem., 37* (1989) 99; W.H. Armstrong, in V.L. Pecoraro (ed.), *Manganese Redox Enzymes,* VCH, New York, 1992, p. 261.

[6] R.T. Stibrany and S.M. Gorun, *Angew. Chem., Int. Ed. Engl., 29* (1990) 1156.

[7] C.J. van Staveren, J. van Eeerden, F.C.J.M. van Veggel, S. Harkema and D.N. Reinhoudt, *J. Am. Chem. Soc., 110* (1988) 4994.

[8] E.S. Yang, M.S. Chan and A.C. Wahl, *J. Phys. Chem., 79* (1975) 2049.

[9] D.D. Perrin and W.L.F. Armarego, *Purification of Laboratory Chemicals,* Pergamon, Oxford, UK, 3rd edn., 1988.

[10] Y. Ciringh, C. Liu and C.P. Horwitz, unpublished results.

[11] L.J. Boucher and D.R. Herrington, *Inorg. Chem., 13* (1974) 1105; L.J. Boucher and C.G. Coe, *Inorg. Chem., 15* (1976) 1334; *14* (1975) 1289; L.J. Boucher and M.O. Farrell, *J. Inorg. Nucl. Chem., 35* (1973) 3731; B. Bosnich, *J. Am. Chem. Soc., 90* (1968) 627.

[12] A. Giacomelli, T. Rotunno and L. Senatore, *Inorg. Chem., 24* (1985) 1303.

[13] Y. Inoue, Y. Liu and T. Hakushi, in Y. Inoue and G.W. Goekel (eds.), *Cation Binding by Macrocycles,* Marcel Dekker, New York, 1990, Ch. 1, p. 1.

[14] B.R. Serr, K.A. Andersen, C.M. Elliot and O.P. Anderson, *Inorg. Chem., 27* (1988) 4499.

[15] P.D. Beer, *Adv. Inorg. Chem., 39* (1992) 79.

[16] F.C.J.M. van Veggel, S. Harkema, M. Bos, W. Verboom, C.J. van Staveren, G.J. Gerritsma and D.N. Reinhoudt, *Inorg. Chem., 28* (1989) 1133; F.C.J.M. van Veggel, M. Bos, S. Harkema, H. van de Bovenkamp, W. Verboom, J. Reedijk and D.N. Reinhoudt, *J. Org. Chem., 54* (1989) 2351; F.C.J.M. van Veggel, S. Harkema, M. Bos, W. Verboom, G.K. Woolthuis and D.N. Reinhoudt, *J. Org. Chem., 56* (1991) 225.

[17] G.C. Dailey, C.P. Horwitz and C.A. Lisek, *Inorg. Chem., 31* (1992) 5325.

[18] C.P. Horwitz, P.J. Winslow, J.T. Warden and C.A. Lisek, *Inorg. Chem., 32* (1993) 82.

[19] C.P. Horwitz, Y. Ciringh, C. Liu and S. Park, *Inorg. Chem., 32* (1993) 5951.

[20] J.W. Gohdes and W.H. Armstrong, *Inorg. Chem., 31* (1992) 368.

[21] E.J. Larson, M.S. Las, X. Li, J.A. Bonadies and V.L. Pecoraro, *Inorg. Chem., 31* (1992) 373.

[22] K. Nakamoto, *Coord. Chem. Rev., 100* (1990) 363; D.M. Kurtz, Jr., *Chem. Rev., 90* (1990) 585.

[23] J.E. Huheey, E.A. Keiter and R.L. Keiter, *Inorganic Chemistry,* Harper Collins, New York, 4th edn., 1993, Ch. 11, p. 405.

[24] C.P. Horwitz, G.C. Dailey and F.S. Tham, *Acta Crystallogr.,* submitted for publication.

[25] S.C. Lee and R.H. Holm, *Inorg. Chem., 32* (1993) 4745.

[26] C.P. Horwitz and S. Weintraub, unpublished results.

[27] G.C. Dailey and C.P. Horwitz, *Inorg. Chem., 31* (1992) 3693.

[28] R.H. Holm, *Chem. Rev., 87* (1987) 1401.

[29] L.K. Woo, *Chem. Rev., 93* (1993) 1125.

[30] K. Wieghardt, U. Bossek, B. Nuber, J. Weiss, J. Bonvoisin, M. Corbella, S.E. Vitols and J.-J. Girerd, *J. Am. Chem. Soc., 110* (1988) 7398; K. Wieghardt, U. Bossek, J. Bonvoisin, P. Beauvillain, B. Nuber, J.-J. Girerd, J. Weiss and J. Heinze, *Angew. Chem., Int. Ed. Engl., 25* (1986) 1030.

[31] K. Wieghardt, U. Bossek, D. Ventur and J. Weiss, *J. Chem. Soc., Chem. Commun.,* (1985) 347.

[32] K. Yamamoto, K. Oyaizu, N. Iwasaki and E. Tsuchida, *Chem. Lett.,* (1993) 1223.

[33] A.J. Bard and L.R. Faulkner, *Electrochemical Methods,* Wiley, New York, 1980.

[34] J.D. Dunitz and L.E. Orgel, *Chem. Soc. London,* (1953) 2595.

[35] C. Sudha, S.K. Mandal and A.R. Chakravarty, *Inorg. Chem., 32* (1993) 3801.

[36] R.H. Heistand II, A.L. Roe and L. Que, Jr., *Inorg. Chem., 21* (1982) 676.

[37] C.J. Boreham and B. Chiswell, *Inorg. Chim. Acta, 24* (1977) 77.

[38] V.V. Zelentsov and I.K. Somova, *Russ. J. Inorg. Chem., 18* (1973) 1125.

[39] S.R. Miller, D.A. Gustowski, Z.C. Chen, G.W. Gokel, L. Echegoyen and A.E. Kaifer, *Anal. Chem., 60* (1988) 2021.